

# Efficient amplification of mid- to far-infrared pulses due to optical pulse conversion in waveguiding quantum-well heterostructures

V. A. Kukushkin\*

*Institute of Applied Physics of RAS, 46 Ulyanov street, 603950 Nizhny Novgorod, Russia*

(Received 5 November 2006; published 20 August 2007)

A method is suggested of efficient mid- to far-infrared (ir) pulse amplification via driving optical pulse energy conversion in waveguiding quantum well (QW) heterostructures at room temperature. It is based on the optical pulse creating transient population inversion at a long-wavelength transition in the three-level scheme formed by QW levels of dimensional quantization. As a result, efficient amplification of a weak mid- to far-ir pulse, propagating simultaneously with the driving one, becomes possible. A waveguide and QW heterostructure design that is optimal for optical-long-wavelength pulse conversion is proposed and shown to be much simpler than that used in quantum cascade lasers. For the typical input peak power of a picosecond driving pulse and mid- to far-ir pulse of  $\sim 100$  W and  $100\text{--}0.1$  mW, respectively, the present scheme is able to produce output ir pulses with peak powers of at least several tens of watts or several tens of milliwatts in the mid- or far-ir range, respectively, i.e., to convert an appreciable part of the optical pulse energy into the mid-ir signal.

DOI: [10.1103/PhysRevA.76.023817](https://doi.org/10.1103/PhysRevA.76.023817)

PACS number(s): 42.55.Px

## I. INTRODUCTION

The generation of powerful short pulses in the mid- to far-infrared (ir) wavelength range is an important problem of modern optics and laser physics, due to increasing need for intense coherent emission in this frequency domain for fundamental investigations and various applications, such as nondestructive evaluation of nonconductive materials [1] and biological tissues [2], molecular spectroscopy [3], studies of surface plasmon-polariton waves [4], coherent control of subband transitions in semiconductor nanostructures [5,6], modulation of optical radiation at far-ir frequencies [7], etc.

There are many different methods proposed so far to produce mid- or far-ir or terahertz radiation, among which are photoconduction [8,9], ultrafast charge transport near a semiconductor surface [10], high- $T_c$  superconducting bridges [11], transition radiation [12], Čerenkov radiation [13], etc. Nevertheless, low-dimensional semiconductor heterostructures [such as quantum wells (QWs) and quantum dots] remain some of the most efficient and convenient devices to generate electromagnetic emission in this frequency range. The main causes are, first, that the transition frequencies between their levels of dimensional quantization can be easily changed by adjusting the structure parameters, and typically correspond to wavelengths from several to hundreds of micrometers, and, second, that simple injection pumping may be employed for them. Unfortunately, free-carrier absorption and diffraction in such devices lead to strong nonresonant losses of mid- and far-ir radiation which rapidly rise with wavelength growth. This circumstance makes lasing in these structures possible only in the presence of a gain large enough to overcome losses. However, due to the very short lifetime of the excited state, the maintenance of high population inversion at low-frequency intersubband transitions is by no means an easy task. This problem can be solved, for

example, by quick depletion of the lower lasing state via stimulated interband recombination [14–16] or phonon emission [17]. As a result of these studies, quantum cascade lasers (QCLs) were realized [18–20], where the lower lasing state is depopulated via tunneling in the superlattice or transition to lower levels with longitudinal optical (LO) phonon emission. But such devices are based on rather complicated multilayer heterostructures and, as a rule, work at low temperatures.

It seems possible, however, to obtain high enough population inversion of the upper lasing state in a pulsed regime on a time scale smaller than its lifetimes due to carrier-carrier scattering,  $\approx 5$  ps [21], or LO phonon emission,  $\sim 1$  ps [22], or impurity scattering,  $\sim 4\text{--}5$  ps [23], or interface roughness scattering,  $4\text{--}50$  ps (for wide  $150\text{--}250$  Å QWs of interest, as shown in Sec. III) [25].<sup>1</sup> It can be realized, for example, in a QW containing a three-level scheme of the states of dimensional quantization where a strong optical exciting pulse equalizes populations of the ground and upper lasing states, thereby creating population inversion between the upper and lower lasing states separated by a mid- to far-ir frequency. So such a structure can work as an efficient amplifier for a long-wavelength pulse propagating simultaneously with the exciting one and having approximately the same duration. As will be shown below, this device can be realized on the basis of a QW heterostructure much simpler than those needed for QCL fabrication, and can work at room temperature. In addition, in such a scheme, free carriers are present in thin QW layers only so that their average density is much smaller than that in QCLs. This results in significantly lower losses for mid- or far-ir field and therefore notably favors their generation. Of course, this device effectiveness depends on the availability of powerful enough driving and long-wavelength

<sup>1</sup>As the interface roughness scattering lifetime for wide QWs being considered here is larger than those due to LO phonon emission or impurity scattering, in what follows I shall take into account only the two latter scattering mechanisms.

\*vakuk@appl.sci-nnov.ru

input pulses. Both of them can be obtained as the output of a nonlinear difference-frequency mixing QW heterolaser, proposed in [26] for continuous-wave (cw) mid- to far-ir generation and considered in [27] in the case of the mode-locking pulsed regime. All one needs to use it as a source of pulses for the present scheme is to remove from its output radiation (by means of a Fabry-Perot filter, for example) the second strong optical pulse resonant with the ground state-lower lasing state transition.

Of course, the practical realization of the method proposed requires a detailed analysis of the optimal QW heterostructure parameters and their dependence on the driving pulse characteristics and amplified wavelength. This is the subject of the present paper. Its structure is as follows. In the next section, I give the mathematical description of a QW waveguiding heterostructure and its interaction with an electromagnetic field. Then I derive the basic equations governing the driving and mid- to far-ir pulse interaction and propagation in such a system. In the third section, I consider the optimal QW waveguiding heterostructure parameters for efficient long-wavelength pulse amplification and give estimates of the maximal gain and output mid- to far-ir pulse peak powers. In conclusion, I cite the main paper results which seem to be the most interesting for experimental implementation.

## II. LONG-WAVELENGTH PULSE AMPLIFICATION IN A QUANTUM-WELL WAVEGUIDING HETEROSTRUCTURE

To ensure efficient long-wavelength pulse amplification due to optical pulse energy conversion, one first of all needs a suitable waveguide, providing pulse confinement and having low absorption coefficients at both wavelengths. These requirements can be satisfied in a single-plasmon waveguide used for mid- to far-ir and THz QCLs [28,29] and modified to also support the optical mode at  $\lambda_1 \approx 0.8 \mu\text{m}$  [30] (Fig. 1). Such a device consists of a conventional slab dielectric waveguide for optical radiation [31] made of a core, say,  $\text{Al}_{0.2}\text{Ga}_{0.8}\text{As}$  layer, sandwiched between two cladding  $\text{Al}_{0.3}\text{Ga}_{0.7}\text{As}$  layers with larger Al mole fraction and therefore a lower refractive index. This structure is covered by a thin metallic layer (made of Au or Pd or other suitable metals or their combinations) on the top, and a thin, heavily doped ( $2 \times 10^{18} \text{ cm}^{-3}$ ) buried layer is introduced between the lower cladding layer and the  $\text{Al}_{0.3}\text{Ga}_{0.7}\text{As}$  semi-insulating substrate. In such a structure, the dielectric waveguide helps to avoid the optical mode penetration into highly conductive layers and its strong absorption there, which is proportional to  $1/\lambda$  [32], and therefore rapidly grows with decreasing wavelength. On the other hand, the mid- to far-ir radiation confinement is provided here through the reflection from the top metallization and formation of an electromagnetic surface wave (surface plasmon) around the buried layer, which has a negative dielectric constant due to high free-carrier density. Although introducing additional absorption due to highly conductive metal and doped layers, such a design provides a much higher confinement factor  $G$  (i.e., the ratio of the power propagating in the active region to the whole beam

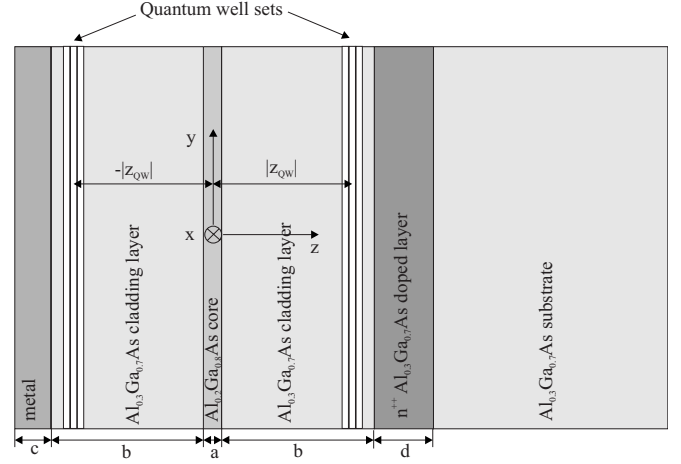


FIG. 1. Schematic of the waveguiding QW heterostructure consisting of an  $\text{Al}_{0.2}\text{Ga}_{0.8}\text{As}$  core and  $\text{Al}_{0.3}\text{Ga}_{0.7}\text{As}$  cladding layers,  $\epsilon_{\text{Al}_{0.2}\text{Ga}_{0.8}\text{As}} > \epsilon_{\text{Al}_{0.3}\text{Ga}_{0.7}\text{As}}$  (a dielectric waveguide), top metallic and highly doped buried  $\text{Al}_{0.3}\text{Ga}_{0.7}\text{As}$  layers (a single-plasmon waveguide), a  $\text{Al}_{0.3}\text{Ga}_{0.7}\text{As}$  semi-insulating substrate, and two QW sets responsible for optical-ir pulse conversion. Here  $c \sim 10\text{--}100 \text{ nm}$ ,  $d \sim 2 \mu\text{m}$ , and the optimal values of parameters  $a$ ,  $b$ , and  $|z_{\text{QW}}|$  are found in Sec. III.

power), for mid- to far-ir fields than do conventional dielectric waveguides, and possesses a large figure of merit  $G/(2 \text{Im} k_2) \lesssim 8.1 \times 10^{-2}$  [29], where  $2 \text{Im} k_2$  is the power long-wavelength absorption coefficient.

Then, let me denote by  $\mathbf{E}_1$  and  $\mathbf{B}_1$  the electromagnetic field of the driving optical pulse and by  $\mathbf{E}_2$  and  $\mathbf{B}_2$  that of the long-wavelength one. Introducing complex amplitudes  $\tilde{\mathbf{E}}_n$  and  $\tilde{\mathbf{B}}_n$ ,  $n = 1, 2$ , one can represent the situation as

$$\left. \begin{array}{l} \mathbf{E}_n \\ \mathbf{B}_n \end{array} \right\} \equiv \frac{1}{2} \times \left\{ \begin{array}{l} \tilde{\mathbf{E}}_n \\ \tilde{\mathbf{B}}_n \end{array} \right\} \times \exp(-i\omega t) + \text{c.c.} \quad (1)$$

$\tilde{\mathbf{E}}_n$  and  $\tilde{\mathbf{B}}_n$  satisfy the Maxwell equations

$$\begin{aligned} \text{rot} \tilde{\mathbf{B}}_n &= -i(\omega_n/c) \epsilon(\omega_n) \tilde{\mathbf{E}}_n + (4\pi/c) \tilde{\mathbf{j}}_n, \\ \text{rot} \tilde{\mathbf{E}}_n &= i(\omega_n/c) \tilde{\mathbf{B}}_n, \end{aligned} \quad (2)$$

where  $\tilde{\mathbf{j}}_n \equiv -i\omega_n \tilde{\mathbf{P}}_n$  are the complex amplitudes of the current densities which are expressed through the complex amplitudes of the corresponding polarizations  $\tilde{\mathbf{P}}_n$ , created on QW interband and intersubband transitions.

Not taking into account unguided radiation modes (which are significantly smaller than those confined inside the waveguide), the complex amplitude of either field can be expanded over the set of waveguide modes  $\mathbf{e}_{nlk}$ ,  $\mathbf{b}_{nlk}$  as [31,33]

$$\tilde{\mathbf{E}}_n = \sum_{lk} \mathcal{E}_{nlk} \mathbf{e}_{nlk}, \quad (3)$$

$$\tilde{\mathbf{B}}_n = \sum_{lk} \mathcal{E}_{nlk} \mathbf{b}_{nlk}, \quad (4)$$

where the index  $l$  stands for the mode polarization ( $l=1$  for a TE mode and  $l=2$  for a TM one), and  $k$  denotes the mode- $x$  wave numbers whose values depend on  $n$  and  $l$ .<sup>2</sup> The modes  $\mathbf{e}_{nlk} \equiv \tilde{\mathbf{e}}_{nlk}(y, z) \exp(ikx)$ ,  $\mathbf{b}_{nlk} \equiv \tilde{\mathbf{b}}_{nlk}(y, z) \exp(ikx)$  satisfy the source-free Maxwell equations

$$\text{rot} \mathbf{b}_{nlk} = -i(\omega_n/c) \boldsymbol{\epsilon}(\omega_n) \mathbf{e}_{nlk}, \quad (5)$$

$$\text{rote}_{nlk} = i(\omega_n/c) \mathbf{b}_{nlk}, \quad (6)$$

and obey the orthogonality condition

$$\frac{c}{4\pi} \int \{[\mathbf{e}_{nlk}, \mathbf{b}_{nl'k'}] - [\mathbf{e}_{nl'k'}, \mathbf{b}_{nlk}]\} \cdot \mathbf{z}^0 dS = \delta_{ll'} \delta_{-kk'} N_{nlk}, \quad (7)$$

where [33]

$$e_{xnl-k}(x, y, z) = -e_{xnlk}(-x, y, z), \quad (8)$$

$$e_{y, znl-k}(x, y, z) = e_{y, znlk}(-x, y, z), \quad (9)$$

$$b_{xnl-k}(x, y, z) = b_{xnlk}(-x, y, z), \quad (10)$$

$$b_{y, znl-k}(x, y, z) = -b_{y, znlk}(-x, y, z), \quad (11)$$

$dS \equiv dy dz$ ,  $\delta_{ij}$  is Kronecker's delta,  $N_{nlk}$  is the norm of the  $nlk$  mode, and, according to this definition,  $N_{nlk} < 0$ .

Following the standard theory of waveguide excitation [33], one can find  $\mathcal{E}_{nlk}$  from the equations

$$d\mathcal{E}_{nlk}/dx = \int \tilde{\mathbf{j}}_n \cdot \mathbf{e}_{nl-k} dS / N_{nlk}. \quad (12)$$

For the further analysis of Eq. (12), I shall bear in mind the typical waveguide design when the whole structure dimension in the transverse  $y$  direction (Fig. 1) is much larger than the core  $\text{Al}_{0.2}\text{Ga}_{0.8}\text{As}$  layer  $z$  width, but does not exceed a value of  $\sim 10 \mu\text{m}$ . Under such parameters, at  $\lambda_1 \approx 0.8 \mu\text{m}$  only one field variation along the  $y$  coordinate is possible in the waveguide, and one can approximate its optical eigenmodes by those of an infinitely wide slab [31,33] so that  $\tilde{\mathbf{e}}_{nlk}$  and  $\tilde{\mathbf{b}}_{nlk}$  depend on  $z$  only. In addition, I shall assume that the core  $\text{Al}_{0.2}\text{Ga}_{0.8}\text{As}$  layer is thin enough (please see the estimates of its optimal thickness in the next section) to support just a couple of optical modes (one TE and one TM). Keeping in mind also the situation, typical for QW laser, when the  $\mathbf{E}_1$  field operates in a TE mode, whereas the  $\mathbf{E}_2$  field is formed by a TM one, in what follows I shall drop the indices  $l, k$  implying them to be  $1, k_1$  for the optical radiation and  $2, k_2$  for the mid- to far-ir signal.

<sup>2</sup>Here I neglect an additional term  $4\pi(\tilde{\mathbf{j}}_n \cdot \mathbf{x}^0)\mathbf{x}^0/[i\omega_n\boldsymbol{\epsilon}(\omega_n)]$ , which should be present in the right-hand side (RHS) of Eq. (3) [33], as, using the QW heterostructure and pulse parameters given below, it can be shown that this term is much smaller than the written one.

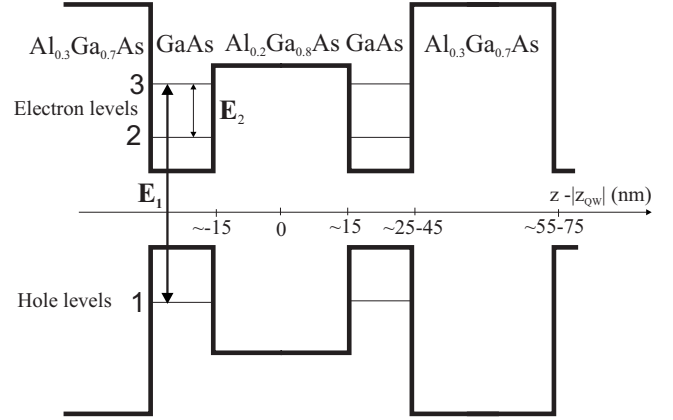


FIG. 2. Effective three-level scheme of electron (hole) QW levels involved in the weak mid- to far-ir pulse ( $\mathbf{E}_2$ ) amplification due to the strong optical pulse ( $\mathbf{E}_1$ ) conversion in the QW set. Along the vertical axis, the lower edge of the conduction band and the upper edge of the valence band of  $\text{Al}_x\text{Ga}_{1-x}\text{As}$ , at the  $\Gamma$  point, are plotted in arbitrary units as functions of the  $z$  coordinate.

Then, to solve Eq. (12), one needs to express  $\tilde{\mathbf{j}}_n \equiv -i\omega_n \tilde{\mathbf{P}}_n$  through  $\mathcal{E}_n$ . This can be done by a detailed consideration of electron and hole dynamics in QWs, which is conducted below.

Let me consider an  $\text{Al}_x\text{Ga}_{1-x}\text{As}$  QW heterostructure consisting of a set of adjacent pairs of wells with each pair consisting of two 10–30 nm thin GaAs layers separated also by a thin spacer ( $\sim 30$  nm) made of  $\text{Al}_{0.2}\text{Ga}_{0.8}\text{As}$  and surrounded by  $\sim 30$  nm thick  $\text{Al}_{0.3}\text{Ga}_{0.7}\text{As}$  layers on each side (Fig. 2). Then, because the GaAs band gap is smaller than those of  $\text{Al}_x\text{Ga}_{1-x}\text{As}$ ,  $x \neq 0$ , levels of dimensional quantization are formed in the GaAs layers. Each level is represented by a subband of electron states distinguished by the projections of electronic quasimomenta on the QW plane,  $p_x, p_y$ . Further, I shall consider a simple structure with one heavy-hole (1) and two electron (2 and 3) states in each QW (Fig. 2).

Of course, all the following consideration can be easily suited for the situation when two hole and one electron QW levels are used [34]. The interband transitions correspond to  $\lambda \sim 0.7\text{--}0.8 \mu\text{m}$ , whereas intersubband transitions lie at  $\lambda \geq 10 \mu\text{m}$  for the electronic levels or even at longer wavelengths  $\geq 70 \mu\text{m}$  for the hole states [26]. It is well known that, when we consider asymmetric QWs with different barrier heights, all three transitions  $2 \rightarrow 1$ ,  $3 \rightarrow 2$ ,  $3 \rightarrow 1$  are dipole allowed, and may have large matrix elements of the order of 0.3–1 nm for interband and 1–3 nm for intersubband transitions [35,36]. It is necessary to mention here that in Fig. 2 and in what follows I do not take into account other long-wavelength transitions that may be present in the QW heterostructure, assuming them to be far enough from resonance with the mid- to far-ir transition  $3 \rightarrow 2$ .

Let me denote by  $\Delta_{31}$  the deviation of the  $3 \rightarrow 1$  transition frequency from  $\omega_1$ ,  $|\Delta_{31}| \ll \omega_1$ , and designate by  $N_{31}$  the corresponding density of  $p_x, p_y$  electronic states in the QW plane whose energy for simplicity's sake is supposed to be a function of  $p_{\parallel} \equiv \sqrt{p_x^2 + p_y^2}$  only (Fig. 3). This axial approximation is rather good for the conduction band where anisotropy

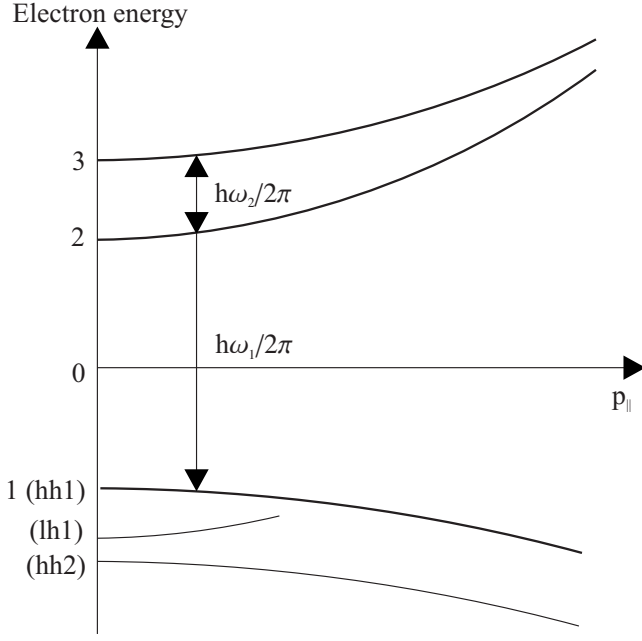


FIG. 3. Schematic of the GaAs band structure near the  $\Gamma$  point with the  $\langle 001 \rangle$  QW growth axis. Here,  $p_{||} \equiv \sqrt{p_x^2 + p_y^2}$  (arbitrary units) and energy (arbitrary units) is counted from the band gap midpoint. The first subband is identified with the first heavy-hole subband (hh1) formed from the  $\Gamma_8$  heavy-hole valence band, the second and third subbands are the two lowest subbands originating in the GaAs  $\Gamma_6$  conduction band. Also shown are the first light-hole (lh1) and the second heavy-hole (hh2) subbands.

manifests itself in terms proportional to electron momentum in the third power only [37], and proves to be reasonable for the valence hole subbands in  $\text{Al}_x\text{Ga}_{1-x}\text{As}/\text{GaAs}/\text{Al}_x\text{Ga}_{1-x}\text{As}$  QWs with the  $\langle 001 \rangle$  growth axis as well [38]. Thus, it is easy to see that, thanks to this assumption,  $\Delta_{31}$  also determines the deviation of the  $3 \rightarrow 2$  frequency from  $\omega_2$ , so that  $\Delta_{31} \equiv \Delta$  and  $N_{31} \equiv N$  can be chosen as the sole parameters to characterize inhomogeneous broadening in such a structure. Hence I shall assume that the frequency of the mid- to far-ir field,  $\omega_2$ , equals the  $3 \rightarrow 2$  frequency at  $\Delta=0$ . Though this assumption is not necessary for further calculations, it seems to be reasonable and allows us to somewhat simplify the following formulas. Similarly to the  $3 \rightarrow 1$  transition, we can introduce the corresponding values  $N_{21}, \Delta_{21}$  and  $N_{32}, \Delta_{32}$  for the  $2 \rightarrow 1$  and  $3 \rightarrow 2$  transitions, which obey the evident equations  $N_{21}\Delta_{21} = N_{32}\Delta_{32} = N\Delta$  and  $\Delta_{32} = \Delta - \Delta_{21}$ . As the third state as a rule has a larger density of states than the second one, these equations result in the conclusion that  $|\Delta| < |\Delta_{21}|$  and, consequently,  $\Delta_{32}, N_{32}$  are opposite to  $\Delta, N$  in sign. On the other hand, as the difference between  $N_{21}$  and  $N$  is not very large, in what follows we shall assume that  $\Delta_{21} \approx \Delta$  and therefore  $|\Delta_{32}| \ll |\Delta|$  as it occurs in QCLs [18,20].

Then, the QW can be described as a three-level system with the density matrix  $\rho_{ij}$  depending on  $\Delta$  only (inhomogeneous broadening). Its nondiagonal elements can be represented as products of the rapid exponential factors with corresponding resonance frequencies  $\omega_{1,2}$  and  $x$  wave numbers  $k_{1,2}$  and slowly varying amplitudes  $\sigma_{ij}$ . The latter can be

found from the system [39] (for the case of low-dimensional heterostructure lasers considered also in [40])

$$\begin{aligned} d\sigma_{21}/dt + \Gamma_{21}\sigma_{21} &= -ie_1\sigma_{32}^* + ie_2^*\sigma_{31}, \\ d\sigma_{31}/dt + \Gamma_{31}\sigma_{31} &= ie_1n_{13} + ie_2\sigma_{21}, \\ d\sigma_{32}/dt + \Gamma_{32}\sigma_{32} &= ie_1\sigma_{21}^* + ie_2n_{23}, \end{aligned} \quad (13)$$

where

$$\begin{aligned} \Gamma_{21} &= \gamma_{21} + i\Delta, \\ \Gamma_{31} &= \gamma_{31} + i\Delta, \\ \Gamma_{32} &= \gamma_{32} - i\eta\Delta, \end{aligned} \quad (14)$$

$n_{ij} = \rho_{ii} - \rho_{jj}$  are population differences,  $e_1 \equiv \mathcal{E}_1 \mathbf{d}_{31} \cdot \mathbf{e}_1 / (2\hbar)$  and  $e_2 \equiv \mathcal{E}_2 \mathbf{d}_{32} \cdot \mathbf{e}_2 / (2\hbar)$  the Rabi frequencies of the optical and mid- to far-ir fields. The ratio of mid- to far-ir and optical detunings,  $\eta \equiv -\Delta_{32}/\Delta$ , according to what has been said above, is positive and much smaller than unity,  $0 < \eta \ll 1$ . To further simplify formulas it will be assumed that the relaxation rates at all transitions between levels 1, 2, and 3 are the same,  $\gamma_{21} = \gamma_{31} = \gamma_{32} \equiv \gamma$ .

In what follows, I shall assume that the mid- to far-ir field is much smaller than the optical one, and employ a perturbation theory over a small parameter  $|\mathcal{E}_2|/|\mathcal{E}_1| \ll 1$ , retaining everywhere terms proportional to the zeroth and first powers of  $\mathcal{E}_2$  only. Then, as the pump and long-wavelength field pulse durations are larger than (or, at least, of the same order as; please see the next section for details) the relaxation time,  $\sim 1/\gamma$ , for estimates of the long-wavelength power one can use the stationary solutions of Eqs. (13), which read as follows:

$$\sigma_{31} = ie_1 n_{13} / \Gamma_{31}, \quad (15)$$

$$\sigma_{32} = ie_2 \frac{n_{23} - n_{13} |e_1|^2 / (\Gamma_{31}^* \Gamma_{21}^*)}{\Gamma_{32} + |e_1|^2 / \Gamma_{21}^*}. \quad (16)$$

According to Eqs. (15) and (16), to obtain the explicit frequency dependence of  $\sigma_{31}$  and  $\sigma_{32}$  one needs to find the diagonal density matrix elements, which are determined from the equations [39,40]

$$d\rho_{11}/dt + r_1(\rho_{11} - \bar{\rho}_{11}) = -2 \text{Im}(e_1^* \sigma_{31}),$$

$$d\rho_{22}/dt + r_2(\rho_{22} - \bar{\rho}_{22}) = -2 \text{Im}(e_2^* \sigma_{32}),$$

$$d\rho_{33}/dt + r_3(\rho_{33} - \bar{\rho}_{33}) = 2 \text{Im}(e_1^* \sigma_{31}) + 2 \text{Im}(e_2^* \sigma_{32}). \quad (17)$$

Further, I shall assume that  $r_1 = r_3 = r$  and, as all the times being considered are shorter than the  $3 \rightarrow 2$  relaxation time,

put  $\rho_{22}=0$ .<sup>3</sup> This considerably simplifies the following formulas, allowing us to derive from Eq. (17) relations for the two population differences  $n_{13}$  and  $n_{23}$  which enter Eqs. (15) and (16):

$$\frac{dn_{13}}{dt} + r(n_{13} - \bar{n}_{13}) = -4 \operatorname{Im}(e_1^* \sigma_{31}) - 2 \operatorname{Im}(e_2^* \sigma_{32}), \quad (18)$$

$$\frac{dn_{23}}{dt} + r(n_{23} - \bar{n}_{23}) = -2 \operatorname{Im}(e_1^* \sigma_{31}) - 4 \operatorname{Im}(e_2^* \sigma_{32}). \quad (19)$$

From Eq. (16) it follows that  $\operatorname{Im}(e_2^* \sigma_{32})$  in Eqs. (18) and (19) is proportional to  $|e_2|^2$  at least, and therefore can be neglected in the above-mentioned linear approximation over  $e_2$ . So the stationary solutions of Eqs. (18) and (19) take the form

$$n_{13} = \frac{\bar{n}_{13}}{1 + 4(\gamma/r)|e_1|^2/(\gamma^2 + \Delta^2)}, \quad (20)$$

$$n_{23} = \bar{n}_{23} - \frac{2(\gamma/r)|e_1|^2 \bar{n}_{13}}{4(\gamma/r)|e_1|^2 + \gamma^2 + \Delta^2}, \quad (21)$$

and then are substituted into Eqs. (15) and (16), which gives the explicit frequency dependence of  $\sigma_{31}$  and  $\sigma_{32}$ . In connection with the last formula, it is worth mentioning that the inversion on the  $3 \rightarrow 2$  transition is maximal within the interval  $|\Delta| \approx \sqrt{4(\gamma/r)|e_1|^2 + \gamma^2}$ , which therefore gives the effective spectral width where efficient amplification of the mid- to far-ir signal takes place.

Then, the complex amplitudes of polarization at the  $3 \rightarrow 1$  and  $3 \rightarrow 2$  transitions can be written as

$$\tilde{\mathbf{P}}_1 = \mathbf{d}_{13} \int_{-\infty}^{+\infty} N \sigma_{31} d\Delta + \text{c.c.}, \quad (22)$$

$$\tilde{\mathbf{P}}_2 = \mathbf{d}_{23} \int_{-\infty}^{+\infty} N \sigma_{32} d\Delta + \text{c.c.} \quad (23)$$

To use these formulas, one needs to concretize the frequency dependence of the quasiequilibrium values of the intersubband population differences  $\bar{n}_{13}$  and  $\bar{n}_{23}$  in Eqs. (20) and (21). As I consider the density matrix evolution over times less than the relaxation time between the third and second subbands, these values should be obtained from Fermi distributions of electrons in the third and first subbands, with instantaneous electron numbers and mean energies in either of them and zero occupancy of the second subband. Nevertheless, according to [21,41] for a  $\sim 10$  nm wide QW the subband quasiequilibrium filling becomes comparable with unity, and Pauli blocking begins to play an appreciable role only for excited electron area densities in the third subband  $\geq 2 \times 10^{11} \text{ cm}^{-2}$ . As will be discussed in the next section, the

<sup>3</sup>In connection with this assumption, it is worth noting that the spectral widths of the optical pulses considered in the next section are much smaller than the  $3 \rightarrow 2$  transition frequencies, so that the pump interaction with the  $2 \rightarrow 1$  transition is nonresonant and, therefore, does not lead to appreciable population of the second subband on the time scale of the optical pulse duration.

optimal amplification densities for a mid- to far-ir field lie well below this value, and therefore one can neglect the small differences between  $\bar{n}_{13}$  and 1 as well as between  $\bar{n}_{23}$  and 0 in Eqs. (18) and (19) for the case of the saturating optical field  $|e_1| \geq \gamma$ ,<sup>4</sup> when, as follows from the results of the numerical analysis described in Sec. III, practically all the long-wavelength gain is acquired.

It is necessary to note here that, as optical or long-wavelength field variations over a QW are negligible, all the above considerations can be easily adapted for the case of several adjacent QWs, by multiplication of the RHS of Eqs. (22) and (23) by the overall QW number  $q$ . According to Fig. 1, this number is equally divided between the two QW sets situated symmetrically with respect to the waveguide core layer.

Using Eqs. (22) and (23), the definition  $\tilde{\mathbf{j}}_n \equiv -i\omega_n \tilde{\mathbf{P}}_n$ , and Eq. (12), one can determine the distance dependence of the field amplitudes  $\mathcal{E}_n$ . Let me start from the optical field, for which Eq. (12) takes on the form

$$d\mathcal{E}_1/dx = -\alpha_1 \mathcal{E}_1 / \sqrt{1 + |\mathcal{E}_1/\mathcal{E}_{1s}|^2}, \quad (24)$$

where  $\mathcal{E}_{1s} \equiv \sqrt{\gamma \hbar} / [\mathbf{d}_{31} \cdot \mathbf{e}_1(x, z_{\text{QW}})]$  is the saturation amplitude,

$$\alpha_1 \equiv -\pi q \omega_1 N S_{\text{QW}} |\mathbf{d}_{31} \cdot \tilde{\mathbf{e}}_1(z_{\text{QW}})|^2 / (2\hbar N_1) \quad (25)$$

is the nonsaturated absorption coefficient for the  $\mathbf{E}_1$  field due to QWs,  $S_{\text{QW}}$  is the QW area in the  $yz$  plane,  $z_{\text{QW}}$  is the  $z$  coordinate of the left or right QW set center (Fig. 1), and, due to the optical mode symmetry,  $\tilde{\mathbf{e}}_1(z_{\text{QW}}) = \tilde{\mathbf{e}}_1(-z_{\text{QW}})$ . If the absolute value of the optical field initial amplitude,  $|\mathcal{E}_1(0)|$ , is significantly larger than  $|\mathcal{E}_{1s}(0)|$ , then from Eq. (24) it is obvious that  $|\mathcal{E}_1/\mathcal{E}_{1s}|$  becomes of the order of unity at a distance  $x_s$ ,

$$x_s \sim \ln \left( \frac{|\mathcal{E}_1(0)/\mathcal{E}_{1s}(0)| + \alpha_1 / \operatorname{Im} k_1}{\sqrt{2} + \alpha_1 / \operatorname{Im} k_1} \right) / \operatorname{Im} k_1, \quad (26)$$

and then drops exponentially over a distance  $\sim 1/\alpha_1$ . If  $|\mathcal{E}_1(0)|$  is much smaller than  $|\mathcal{E}_{1s}(0)|$ , then the optical field evolution from the very beginning is an exponential decrease, with a decrease equal to  $\alpha_1$ .

Now let me turn to the equation for the long-wavelength field amplitude  $\mathcal{E}_2$ . In analogy with the above-outlined derivation for the optical field, I get

<sup>4</sup>This condition means that the quasienergy structure of the  $3 \rightarrow 1$  transition can be resolved. But this structure exists for a time interval of the order of  $1/\gamma$  while the Rabi oscillations is not damped yet [42]. As the overall optical pulse duration is larger than  $1/\gamma$ , it means that for the most part this structure disappears, and the mid- to far-ir pulse amplification indeed has quasistationary character.

$$\frac{d\mathcal{E}_2}{dx} = \frac{\alpha_2 \mathcal{E}_2 |\mathcal{E}_1/\mathcal{E}_{1s}|^2 [4 + 4\sqrt{1 + |\mathcal{E}_1/\mathcal{E}_{1s}|^2} + 2|\mathcal{E}_1/\mathcal{E}_{1s}|^2 - (r/\gamma)|\mathcal{E}_1/\mathcal{E}_{1s}|^2]}{4[(1 + \eta\sqrt{1 + |\mathcal{E}_1/\mathcal{E}_{1s}|^2})(1 + \sqrt{1 + |\mathcal{E}_1/\mathcal{E}_{1s}|^2}) + r|\mathcal{E}_1/\mathcal{E}_{1s}|^2/(4\gamma)]\sqrt{1 + |\mathcal{E}_1/\mathcal{E}_{1s}|^2}(1 + \sqrt{1 + |\mathcal{E}_1/\mathcal{E}_{1s}|^2})(2\gamma/r - 1)}, \quad (27)$$

where

$$\alpha_2 \equiv -\pi q \omega_2 (2\gamma/r - 1) N S_{QW} |\mathbf{d}_{32} \cdot \tilde{\mathbf{e}}_2(z_{QW})|^2 / (2\hbar N_2), \quad (28)$$

and, due to the large extent of the mid- to far-ir mode, I neglect the difference between  $\tilde{\mathbf{e}}_2(z_{QW})$  and  $\tilde{\mathbf{e}}_2(-z_{QW})$ .

Though rather cumbersome, Eq. (27) can be substantially simplified by employing the following consideration. First of all, it is clear that for  $\eta \ll 1/4$  one can neglect the term  $\eta\sqrt{1 + |\mathcal{E}_1/\mathcal{E}_{1s}|^2}$  in its denominator for any value of the ratio  $|\mathcal{E}_1/\mathcal{E}_{1s}|$ . The inequality  $\eta \ll 1/4$  is indeed the case for an  $\text{Al}_x\text{Ga}_{1-x}\text{As}/\text{GaAs}/\text{Al}_x\text{Ga}_{1-x}\text{As}$  QW [Eq. (35) below]. Then, let me consider separately two cases, namely, when the initial optical field is much larger or much smaller than its beginning saturation value, i.e., when  $|\mathcal{E}_1(0)/\mathcal{E}_{1s}(0)| \gg 1$  or  $|\mathcal{E}_1(0)/\mathcal{E}_{1s}(0)| \ll 1$ . In the first case, from Eq. (27), one obtains that, while  $|\mathcal{E}_1/\mathcal{E}_{1s}| > 1$ , i.e., while  $x \leq x_s$ ,

$$d\mathcal{E}_2/dx \approx \alpha_2 \mathcal{E}_2, \quad (29)$$

and  $\mathcal{E}_2$  grows exponentially up to the distance  $\sim x_s$  where the absolute value of the long-wavelength field complex amplitude,  $|\tilde{\mathbf{E}}_2| = |\mathcal{E}_2 \mathbf{e}_2|$ , reaches a value of

$$\frac{|\tilde{\mathbf{E}}_2(x_s)|}{|\tilde{\mathbf{E}}_2(0)|} \sim \exp[(\alpha_2 - \text{Im } k_2)x_s]. \quad (30)$$

The independence of the mid- to far-ir field amplification rate Eq. (29) from the pump power for  $|\mathcal{E}_1/\mathcal{E}_{1s}| > 1$  (i.e., when the optical field intensity exceeds the saturation value) can be intuitively understood from the following considerations. For  $|\mathcal{E}_1/\mathcal{E}_{1s}| > 1$ , the strong pump equalizes the populations of the first and third levels in the interval  $|\Delta| \leq |e_1|$  near the pump central frequency. As a result, the level population differences  $n_{13} \propto 1/|e_1|^2$  [Eq. (20)] and  $n_{23} \approx -1/2$  [Eq. (21)] in this interval, and  $n_{13} \approx -1$ ,  $n_{23} \propto 1/|\Delta|^2$  outside it. Having substituted them into Eq. (16) for  $\sigma_{32}$ , one can see that the latter (as a function of  $\Delta$ ) is maximal in intervals with widths of the order of  $|e_1|$  around  $\Delta \sim \pm |e_1|$ , where it scales as  $1/|e_1|$ , and drops as  $1/|e_1|^2$  and  $1/\Delta^2$  for smaller or larger  $|\Delta|$ , respectively. So these intervals determine the integral from  $\sigma_{32}$  over  $\Delta$  in Eq. (23) which therefore becomes independent of the pump field intensity for  $|\mathcal{E}_1/\mathcal{E}_{1s}| > 1$ . According to the above derivation, it leads to the independence of the mid- to far-ir field growth rate from the pump power as well.

For  $x > x_s$ , the value  $|\mathcal{E}_1/\mathcal{E}_{1s}|$  becomes smaller than unity so that Eq. (27) reduces to the formula

$$d\mathcal{E}_2/dx \approx \frac{\alpha_2 \mathcal{E}_2 |\mathcal{E}_1/\mathcal{E}_{1s}|^2}{2(2\gamma/r - 1)}, \quad (31)$$

which approximately joins at  $x \sim x_s$  with Eq. (29) (taking into account that in the considered scheme  $\gamma \sim r$  [40]). Then, from Eq. (31) it follows that at  $x > x_s$  the mid- to far-ir field increases with  $x$  up to  $x = x_g$  only,

$$x_g \sim x_s + \frac{\ln[(2\gamma/r - 1)\text{Im } k_2/\alpha_2]^{-1}}{2(\alpha_1 + \text{Im } k_1)}; \quad (32)$$

for  $x > x_g$  the long-wavelength field growth rate  $\alpha_2 |\mathcal{E}_1/\mathcal{E}_{1s}|^2 / [2(2\gamma/r - 1)] - \text{Im } k_2$  becomes negative, so that  $\mathbf{E}_2$  decreases. The mid- to far-ir field gain over the interval  $x_s < x < x_g$  is given by the formula

$$\frac{|\tilde{\mathbf{E}}_2(x_g)|}{|\tilde{\mathbf{E}}_2(x_s)|} \approx \exp \left[ \frac{\text{Im } k_2}{2(\alpha_1 + \text{Im } k_1)} \left( \frac{\alpha_2}{(2\gamma/r - 1)\text{Im } k_2} - \ln \frac{\alpha_2}{(2\gamma/r - 1)\text{Im } k_2} - 1 \right) \right]. \quad (33)$$

In the second case of small input optical field,  $|\mathcal{E}_1(0)/\mathcal{E}_{1s}(0)| \ll 1$ , the mid- to far-ir field amplification from the very beginning is governed by Eq. (31), and the corresponding gain is given by Eq. (33).

In connection with the approximate solution obtained of the system (24) and (27) and the expressions for the mid- to far-ir field gain, Eqs. (30) and (33), calculated by means of it, it is necessary to note that formulas (30) and (33) are used in the next section as a tool for finding the optimal parameter set for mid- to far-ir field amplification only, and are not suitable for the calculation of the actual gain value. This is because even relatively small mistakes in the powers of exponents in these equations can lead to substantial deviations of these estimates from the true gain value. The other cause is that Eqs. (30) and (33) [as well as Eq. (27), from which they are obtained] do not take into account the effect of the optical field populating the second subband at  $\Delta \approx (0.3 - 1)\omega_2$ , due to electron transitions from the first subband or successive heavy-hole or light-hole subbands lying below the first subband (Fig. 3), and the corresponding mid- to far-ir field absorption at this  $\Delta$  (for a detailed discussion of this effect please, see the next section). So all the estimates of gain and output mid- to far-ir power in Sec. III are made on the basis of the numerical solution of the system (24) and (27), modified so as to include the latter effect, as explained below. The results of these simulations are also shown here in Fig. 4 for the typical system parameters.

It is seen from this figure that the mid- to far-ir field gain for  $\lambda_2 \approx 60 \mu\text{m}$  proves to be more than ten times smaller than that for  $\lambda_2 \approx 22 \mu\text{m}$ , in spite of the tenfold increase in adjacent QW number. This is due to the quick growth of  $|N_2|$

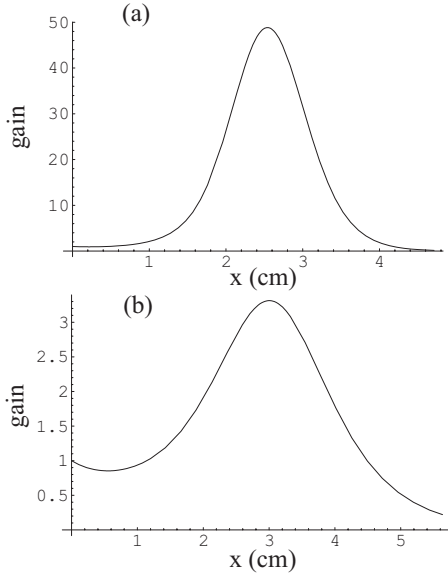


FIG. 4. Total gain for mid- to far-ir field with  $\lambda_2=22 \mu\text{m}$  (a) and  $\lambda_2=60 \mu\text{m}$  (b), resulting from the numerical solution of the system (24) and (27), modified so as to include the mid- to far-ir field absorption at  $\Delta \approx (0.3-1)\omega_2$  (please see discussion below). The parameters used for  $\lambda_2=22 \mu\text{m}$  (please see the next section for details) are the following:  $\text{Im } k_1=0.25 \text{ cm}^{-1}$ ,  $\text{Im } k_2=3.5 \text{ cm}^{-1}$ ,  $q=8$ ,  $\alpha_1=0.15q \text{ cm}^{-1}$ ,  $\alpha_2=1.47q \text{ cm}^{-1}$ ,  $\gamma=10^{12} \text{ c}^{-1}$ ,  $\gamma/r=1$ ,  $|\mathcal{E}_1(0)/\mathcal{E}_{1s}(0)|=6$ , from which  $x_s \sim 2.2 \text{ cm}$  and  $x_g-x_s \sim 0.4 \text{ cm}$ . The same for  $\lambda_2=60 \mu\text{m}$  are  $\text{Im } k_1=0.25 \text{ cm}^{-1}$ ,  $\text{Im } k_2=1.35 \text{ cm}^{-1}$ ,  $q=80$ ,  $\alpha_1=0.012q \text{ cm}^{-1}$ ,  $\alpha_2=0.086q \text{ cm}^{-1}$ ,  $\gamma=2 \times 10^{11} \text{ c}^{-1}$ ,  $\gamma/r=1$ ,  $|\mathcal{E}_1(0)/\mathcal{E}_{1s}(0)|=6$ , from which  $x_s \sim 2.5 \text{ cm}$  and  $x_g-x_s \sim 0.7 \text{ cm}$ .

with the wavelength enhancement, and the corresponding decrease of  $\alpha_2 \propto 1/(|N_2|\lambda_2)$  [Eq. (28)]. The other effect causing such a rapid drop in long-wavelength gain is the reduction of the value  $(0.3-1)\eta\omega_2$  divided by the linewidth of the  $3 \rightarrow 2$  transition (please see the next section for details), and therefore substantial growth of the mid- to far-ir field absorption at  $\Delta \approx (0.3-1)\omega_2$  with decreasing  $\omega_2$ .

In the next section, I consider the optimal structure parameters allowing us to maximize the long-wavelength pulse amplification determined by Eqs. (30) and (33).

### III. OPTIMAL QW HETEROSTRUCTURE AND OPTICAL PULSE PARAMETERS FOR MID- TO FAR-IR PULSE AMPLIFICATION

To consider the optimal parameters of the QW waveguiding heterostructure and exciting pulse providing the maximal possible gain for the long-wavelength field, one needs first to estimate the density of states for the  $3 \rightarrow 1$  transition,  $N$ , and the value  $\eta$  which determine the long-wavelength field amplification. To do so I bear in mind transitions around the  $\Gamma$  point of the GaAs crystal (Fig. 3) with the  $\langle 001 \rangle$  QW growth axis, and identify the first subband with the highest subband formed from the  $\Gamma_8$  heavy-hole valence band [37] (effective mass  $m_1 \approx 0.5m$  [38]; where  $m$  is the free electron mass), whereas the second and third subbands are the two lowest subbands originating in the GaAs  $\Gamma_6$  conduction band [37]

with slightly different effective masses,  $m_2 \lesssim m_3$ , both of them being very close to the GaAs  $\Gamma_6$  effective electron mass  $0.07m$  for the wide QW of interest [43]. Thus, an elementary derivation gives for  $N$  and  $\eta$  the following expressions:

$$N \approx m_1 m_3 [2\pi\hbar(m_1 + m_3)\Delta z_{\text{QW}}], \quad (34)$$

$$\eta = m_1(m_3 - m_2)/[m_2(m_1 + m_3)] \lesssim 0.1, \quad (35)$$

where  $\Delta z_{\text{QW}}$  is the QW width, and the estimate for  $\eta$  has been made using simple analytical formulas for effective electron masses in an infinite QW with a width  $\geq 150 \text{ \AA}$  [43].

It is appropriate to mention here that, though the parameter  $\eta$ , Eq. (35), is quite small and, as was mentioned after Eq. (27), does not influence significantly the long-wavelength growth rate for any optical field amplitude, the fact that  $\eta \neq 0$ , i.e., that the effective electron mass in the third subband,  $m_3$ , is slightly higher than that in the second one,  $m_2$ , Eq. (35), is very important for the following reason. As is clear from Fig. 3, for  $\Delta \approx (0.3-1)\omega_2$ , the optical field populates the second subband due to electron transitions from the first subband or successive heavy-hole or light-hole subbands lying below the first subband. If the second and third subbands were exactly parallel, i.e., if  $\eta \equiv 0$ , this effect could lead to long-wavelength field absorption on the  $2 \rightarrow 3$  transition at  $\Delta \approx (0.3-1)\omega_2$  and completely overcome its amplification on this transition at  $\Delta \approx 0$ . But, fortunately, since  $\eta \neq 0$ , the frequencies of the  $3 \rightarrow 2$  transition at these  $\Delta \approx (0.3-1)\omega_2$  are lower than  $\omega_2$  by  $(0.3-1)\eta\omega_2$ .<sup>5</sup> The latter value for  $\lambda_2 \approx 22$  or  $60 \mu\text{m}$  (please see below) should be compared with the linewidth of the  $3 \rightarrow 2$  transition,  $\gamma + r|\mathcal{E}_1/\mathcal{E}_{1s}|^2/[4(1 + \sqrt{1 + |\mathcal{E}_1/\mathcal{E}_{1s}|^2})]$ , which can be easily obtained from a simple generalization of Eq. (27) for the case when the frequency of the mid- and far-ir field  $\omega_2$  does not equal the  $3 \rightarrow 2$  frequency at  $\Delta=0$ ,  $\omega_{32}$ , i.e., by assuming everywhere in its derivation  $\Gamma_{32} = \gamma_{32} + i(\omega_{32} - \omega_2 - \eta\Delta)$ . The estimates show that, under the optimal  $\gamma \sim r$  and  $|\mathcal{E}_1/\mathcal{E}_{1s}|$  given below, the value  $(0.3-1)\eta\omega_2$  is much larger than the  $3 \rightarrow 2$  transition linewidth, and, therefore, the absorption of the long-wavelength field at these  $\Delta$  is substantially suppressed.

As was mentioned before, to provide efficient long-wavelength pulse amplification, its group velocity has to be equal to that of the optical pulse. As different waveguide modes have diverse group velocities, this condition is difficult to satisfy if optical and mid- to far-ir pulses are formed

<sup>5</sup>It is appropriate to mention here that  $|\eta|$  has larger values for the light- to heavy-hole transition (Fig. 3) due to the strong difference of hole masses in these subbands. So this transition seems rather promising for the long-wavelength pulse amplification with synchronous optical pumping. But, first, the typical corresponding wavelengths  $\lambda_2 \geq 80 \mu\text{m}$  [38], so that it is less appropriate for the range  $10-70 \mu\text{m}$  considered in the paper, and, second, the group velocity at  $\lambda_2 \geq 80 \mu\text{m}$  does not coincide with that of the optical pulse for the waveguide design considered in the paper, so that another, more complicated, heterostructure arrangement is needed for the employment of this transition. Thus, I do not examine this possibility in detail in the present paper.

by several modes. So the waveguide should provide the propagation of just a couple (one TE and one TM) of optical and long-wavelength modes. Then, as the optical and mid- to far-ir input pulses have TE and TM polarizations, respectively, as is typical in QW lasers [26], the polarizations of the driving and long-wavelength pulses inside the waveguiding heterostructure will be the same. Their group velocities can be found from the frequency dependence of the mid- to far-ir and optical mode refractive indices in the waveguide,  $n_2, n_1$ . Taking into account the fact that the optical field is practically fully contained in the confining and cladding layers and does not penetrate into metallic and highly doped ones, one can admit that  $n_1$  is determined by the refractive indices of the confining and cladding layers only. As to the mid- to far-ir pulse, noting that the metallic and highly doped layers are very thin ( $\sim 10$  nm and  $\sim 300$  nm, respectively [29,32]), one can adopt with good accuracy that  $n_2$  is determined by the refractive indices of the confining and cladding layers and the substrate only. For dispersion of the GaAs and AlAs dielectric functions, I shall use fitting formulas [44,45] and approximate  $\epsilon_{\text{Al}_x\text{Ga}_{1-x}\text{As}}$  by the simple formula  $\epsilon_{\text{Al}_x\text{Ga}_{1-x}\text{As}} = x\epsilon_{\text{AlAs}} + (1-x)\epsilon_{\text{GaAs}}$  [46,47]. As the difference between  $\epsilon_{\text{Al}_{0.2}\text{Ga}_{0.8}\text{As}}$  and  $\epsilon_{\text{Al}_{0.3}\text{Ga}_{0.7}\text{As}}$  is very small,  $\lesssim 0.1$  beyond the reststrahlen region, it is sufficient for estimates to approximate the optical and mid- to far-ir mode refractive indices by that of  $\text{Al}_x\text{Ga}_{1-x}\text{As}$  at some intermediate value of  $x$ , say,  $x = 0.25$ .

Then, using standard waveguide theory [31], it is easy to obtain the result that, for the structure parameters found above, the group velocity of the optical pulse with a carrier wavelength of  $\lambda_1 \approx 0.8 \mu\text{m}$  is equal to that of the long-wavelength pulse if its central wavelength  $\lambda_2$  lies about 22 or 60  $\mu\text{m}$ . So only for these two wavelength can the mid- to far-ir pulse amplification can be efficient. Nevertheless, it is important to mention here that, of course, many types of other waveguide designs are possible, so that one can, in principle, match the optical group velocity with the mid- to far-ir one for a wide range of mid- to far-ir carrier wavelengths, thereby providing efficient amplification of a long-wavelength signal at a desirable central frequency.

Further, it is preferable to make the optical field transverse variation as smooth as possible, because this diminishes its change over the QW set and therefore allows each QW to be placed at the optimal point of the optical mode transverse structure. In turn, this means that the absolute value of the optical mode norm  $N_1$  should be as large as possible. The numerical analysis of the standard equations of the dielectric slab waveguide theory [31] shows that this can be realized by either increasing or decreasing the confining layer thickness in comparison with the value of  $\approx 0.3 \mu\text{m}$  when  $|N_1|$  is minimal under the above-mentioned dielectric waveguide composition. On the other hand, the same analysis indicates that the dielectric waveguide supports propagation only of the pair of the optical modes (one TE and one TM) if its confining layer thickness is less than 0.6  $\mu\text{m}$ . So a substantial increase of  $N_1$  can be achieved only by reduction of the confining layer thickness below 0.3  $\mu\text{m}$ . The growth of  $|N_1|$  under diminishing confining layer thickness means that enhancement of the optical mode spreads beyond the confining

layer. It also means that the cladding layer thickness  $2b$  increases to avoid optical mode penetration into the highly conductive layers and its strong absorption there. But the increase of  $2b$  is limited by the condition that this value be much less than the mid- to far-ir mode spread in the substrate. This is because larger  $2b$  leads to the growth of the absolute value of the mid- to far-ir mode norm  $N_2$ , and, according to Eqs. (30) and (33), decrease of the mid- to far-ir gain. The long-wavelength mode spread in the substrate can be obtained by adjusting the results of [29] to the mid- to far-ir wavelengths  $\lambda_2 = 22$  or 60  $\mu\text{m}$  being considered here. So it can be shown that the full width at half maximum (FWHM) of the mid- to far-ir field spread in the substrate is of the order of 13  $\mu\text{m}$  for  $\lambda_2 = 22 \mu\text{m}$  and 65  $\mu\text{m}$  for  $\lambda_2 = 60 \mu\text{m}$ . According to what was said above, the optimal aggregate thickness of the dielectric waveguide in these cases should be  $\sim$  three times less than these figures and therefore I obtain  $b \approx 2$  and 10  $\mu\text{m}$ , respectively, for the mentioned wavelengths. Under such parameters, to ensure optical field isolation from the highly conductive and therefore absorbing layers, its FWHM transverse spread should be  $\sim 1.3$  and 6  $\mu\text{m}$ , respectively. As a simple numerical analysis shows, this is indeed the case if the confining layer thickness is  $a \approx 0.12$  and 0.024  $\mu\text{m}$  for  $\lambda_2 = 22$  and 60  $\mu\text{m}$ , respectively.

Then, let me discuss the optimal values of QW-mode coupling for the mid- to far-ir signal,  $|\mathbf{d}_{32} \cdot \tilde{\mathbf{e}}_2(z_{\text{QW}})|$ , and the optical field,  $|\mathbf{d}_{31} \cdot \tilde{\mathbf{e}}_1(z_{\text{QW}})|$ . A simple analytical analysis of Eqs. (26) and (30) shows that the gain is maximal if  $|\mathbf{d}_{32} \cdot \tilde{\mathbf{e}}_2(z_{\text{QW}})|$  is also maximal because of growth of  $\alpha_2 \propto |\mathbf{d}_{32} \cdot \tilde{\mathbf{e}}_2(z_{\text{QW}})|^2$ . As to the value  $|\mathbf{d}_{31} \cdot \tilde{\mathbf{e}}_1(z_{\text{QW}})|$ , the same analysis shows that its optimum corresponds to such an excited electron density in the third subband,  $\rho_3 \equiv \int N \rho_{33} d\Delta$ , that the relaxation time due to electron-electron scattering inside the first and third subbands,  $1/\gamma \sim 1/r$  [40], is of the order of the relaxation time between third and second subbands,  $\tau_{32}$ , thanks to electron interaction with phonons or impurities. Larger  $|\mathbf{d}_{31} \cdot \tilde{\mathbf{e}}_1(z_{\text{QW}})|$  leads to higher excited electron density in the third subband and therefore larger  $\gamma \sim r$  (which are proportional to  $\rho_3$  for the small occupational numbers being considered). This, in turn, causes the increase of the  $3 \rightarrow 2$  linewidth,  $\gamma + r |\mathcal{E}_1/\mathcal{E}_{1s}|^2 / [4(1 + \sqrt{1 + |\mathcal{E}_1/\mathcal{E}_{1s}|^2})]$ , above the value  $(0.3-1)\omega_2\eta$ , and therefore long-wavelength field efficient absorption on the  $3 \rightarrow 2$  transition at  $\Delta \approx (0.3-1)\omega_2$ . On the other hand, smaller  $|\mathbf{d}_{31} \cdot \tilde{\mathbf{e}}_1(z_{\text{QW}})|$  results in lower excited electron density in the third subband and, as follows from the numerical analysis of Eqs. (30) and (33) with the parameters given below, smaller long-wavelength gain at the  $3 \rightarrow 2$  transition near  $\Delta = 0$ . Let me note here that, as the relaxation time between the third and second subbands due to electron-electron scattering is typically ten times larger than  $1/\gamma \sim 1/r$  [48], for optimal  $|\mathbf{d}_{31} \cdot \tilde{\mathbf{e}}_1(z_{\text{QW}})|$ , i.e., under the condition  $1/\gamma \sim 1/r \sim \tau_{32}$ ,  $\tau_{32}$  is indeed determined by electron interaction with phonons or impurities, and is not influenced by electron-electron collisions in the third subband.

So, for a given  $\mathcal{E}_1(0)$ , the actual value of  $|\mathbf{d}_{31} \cdot \tilde{\mathbf{e}}_1(z_{\text{QW}})|$  can be found from the condition  $\tau_{32} = 1/\gamma(\rho_3)$ , where the function  $\gamma(\rho_3)$  can be estimated using data from [21] for the  $3 \rightarrow 2$  relaxation time due to electron-electron scattering, and tak-

ing into account that  $1/\gamma$  is typically ten times smaller than this value [48]. The excited electron density  $\rho_3$  in the essential frequency interval of the  $3 \rightarrow 2$  transition responsible for the mid- to far-ir signal amplification,  $|\Delta| \lesssim \sqrt{4(\gamma/r)|e_1|^2 + \gamma^2}$ , can be obtained from Eq. (21) combined with the fact that for times much smaller than the  $3 \rightarrow 2$  relaxation time,  $\rho_{22} \approx 0$ :

$$\rho_3 = \frac{\pi N \gamma |\mathcal{E}_1 / \mathcal{E}_{1s}|^2}{2\sqrt{1 + |\mathcal{E}_1 / \mathcal{E}_{1s}|^2}}. \quad (36)$$

In the case when  $\lambda_2 \approx 22 \mu\text{m}$ , the value  $\omega_2$  is larger than the LO phonon frequencies in GaAs and AlAs [49], so that at the optimal  $|\mathbf{d}_{31} \cdot \tilde{\mathbf{e}}_1(z_{\text{QW}})|$  the value  $\tau_{32}$  is determined by LO phonon emission and lies around 1 ps [22]. Then, following what has been said above, I get the optimal excited electron density  $\rho_3^{\text{opt}} \approx 6.5 \times 10^{16} \text{ cm}^{-3}$  in a 150 Å wide QW, which corresponds to  $|\mathcal{E}_1(0)/\mathcal{E}_{1s}(0)| \approx 6$  [Eq. (36)].

In the case when  $\lambda_2 \approx 60 \mu\text{m}$ , the frequency  $\omega_2$  is smaller than the LO frequencies for both GaAs and AlAs, so that the  $3 \rightarrow 2$  relaxation time is determined by impurity scattering, which is of the order of 4–5 ps at 300 K for an  $\text{Al}_x\text{Ga}_{1-x}\text{As}/\text{GaAs}/\text{Al}_x\text{Ga}_{1-x}\text{As}$  QW [23]. On the analogy of the previous case, I obtain the optimal excited electron density  $\rho_3^{\text{opt}} \approx 8 \times 10^{15} \text{ cm}^{-3}$  in a 265 Å wide QW, which determines the ratio  $|\mathcal{E}_1(0)/\mathcal{E}_{1s}(0)| \approx 6$  [Eq. (36)].

It is worth noticing here that, at the optimal densities of carriers in QWs obtained above, their interaction cannot be ignored. Nevertheless, though neglecting this issue, the simple three-level scheme employed here allows qualitatively valid results for the fields' behaviors in the considered situation to be obtained. This statement can be supported by an estimate of the relative correction to the frequency of the  $3 \rightarrow 2$  transition due to many-body effects treated in the macroscopic Hartree field approach. Corresponding calculations, based on the results of [24] and employing the above-cited optimal parameters, give a value of  $\sim 10\%$  in the case of mid- to far-ir emission amplification at  $\lambda_2 \approx 22 \mu\text{m}$ , and  $\sim 30\%$  at  $\lambda_2 \approx 60 \mu\text{m}$ . So the three-level model seems to be quite adequate for making qualitative conclusions here. However, as these shifts are larger than the  $3 \rightarrow 2$  linewidth  $\gamma + r|\mathcal{E}_1/\mathcal{E}_{1s}|^2/[4(1 + \sqrt{1 + |\mathcal{E}_1/\mathcal{E}_{1s}|^2})]$ , this effect leads to certain conditions determining the optimal carrier frequency of the input mid- to far-ir pulse and its modulation with time. First,  $\omega_2$  at its leading edge should differ from the  $3 \rightarrow 2$  transition frequency at  $\Delta=0$  by the values found above. Second, since it is proportional to the whole excited electron density in the third subband [and not only in the interval  $|\Delta| \lesssim \sqrt{4(\gamma/r)|e_1|^2 + \gamma^2}$ ], this shift changes during the optical pulse. It means that the mid- to far-ir pulse carrier frequency should be modulated. The depth of this modulation can be estimated from the following considerations. The rate of electron sweeping from the interval  $|\Delta| \lesssim \sqrt{4(\gamma/r)|e_1|^2 + \gamma^2}$  into the states of the third subband with larger  $|\Delta|$  due to intrasubband electron-electron collisions is  $\sim \gamma$ . The third subband electron density in the interval  $|\Delta| \lesssim \sqrt{4(\gamma/r)|e_1|^2 + \gamma^2}$  is stationary and given by Eq. (36). Consequently, the whole excited electron density in the third subband left by the optical pulse with duration  $> 1/\gamma$  is approxi-

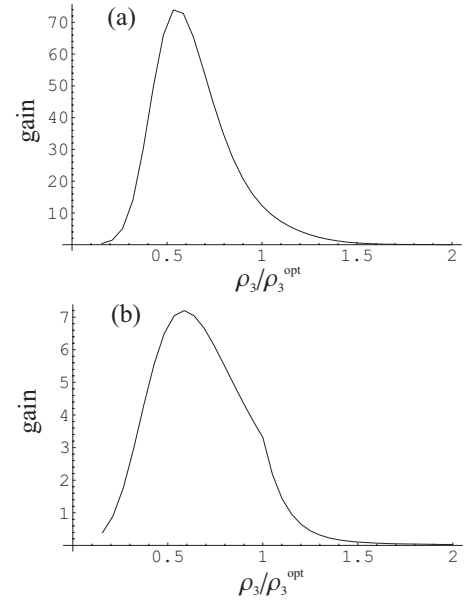


FIG. 5. Total gain for mid- to far-ir field with  $\lambda_2 = 22 \mu\text{m}$  at the point  $x = 1.7 \text{ cm}$  (a) and  $\lambda_2 = 60 \mu\text{m}$  at the point  $x = 3 \text{ cm}$  (b) as a function of the normalized excited electron density  $\rho_3/\rho_3^{\text{opt}}$ , where  $\rho_3^{\text{opt}} \approx 6.5 \times 10^{16} \text{ cm}^{-3}$  for  $\lambda_2 = 22 \mu\text{m}$  and  $\rho_3^{\text{opt}} \approx 8 \times 10^{15} \text{ cm}^{-3}$  for  $\lambda_2 \approx 60 \mu\text{m}$ . This graph represents the results of the numerical solution of the system (24) and (27) [modified so as to include the mid- to far-ir field absorption at  $\Delta \approx (0.3-1)\omega_2$ ] for the same parameters as in Fig. 4 except for  $\gamma$ ,  $|\mathcal{E}_1(0)/\mathcal{E}_{1s}(0)|$ , and  $\alpha_1$ , which vary with density (for fixed pump field initial amplitude).

mately twice the value given by Eq. (36). This means that the shift of the  $3 \rightarrow 2$  transition frequency changes approximately by two times during the optical pulse. This leads to the conclusion that for efficient amplification the input mid- to far-ir pulse should be frequency modulated with the modulation depth  $\sim 10\%$  for  $\lambda_2 \approx 22 \mu\text{m}$  (which corresponds to the pulse spectral width  $\sim 0.1\omega_2$ ) and  $\sim 30\%$  for  $\lambda_2 \approx 60 \mu\text{m}$  (spectral width  $\sim 0.3\omega_2$ ). Alternatively, if there is no input mid- to far-ir pulse at all, and the latter is generated in the active medium (created by the pumping optical pulse) from spontaneous noise, it will have the mentioned frequency modulation.

More precise estimates of the optimal excited electron densities and the gain sensitivity to the deviations from them can be obtained from Fig. 5, showing the results of the numerical solution of the system (24) and (27) modified so as to include the mid- to far-ir field absorption at  $\Delta \approx (0.3-1)\omega_2$ . It shows that the actual optimal densities (i.e., the densities corresponding to the gain maxima in Fig. 5) are about  $3.9 \times 10^{16}$  and  $4.8 \times 10^{15} \text{ cm}^{-3}$  for  $\lambda_2 \approx 22$  and  $60 \mu\text{m}$ , respectively. These corrections to the values  $\rho_3^{\text{opt}}$  found above are quite understandable and due to the approximate analytical procedure for their calculation. From Fig. 5, it is also seen that the gains prove to be rather fast functions of density for both mid- and far-ir wavelengths. So, for  $\lambda_2 \approx 22 \mu\text{m}$ , the gain drops by 14 times with twofold density increase or decrease in comparison with its optimal value. For  $\lambda_2 \approx 60 \mu\text{m}$ , the gain appears to be slightly less sensitive to the density variations, dropping by  $\sim$  ten times for a density

twice as large as the optimal one, and falling by only three times with the same density reduction. Thus, it seems to be rather important for practical realization of the method proposed to work near the optimal excited electron densities in QWs.

In connection with the optimal ratios  $|\mathcal{E}_1(0)/\mathcal{E}_{1s}(0)| \approx 6$  found above, it is necessary to mention that, for typical values of optical transition matrix elements lying about 0.3–1 nm [35,36], they can be achieved even for low input optical peak powers of 4–40 mW, which are much smaller than those already obtained in mode-locked QW heterolasers [50,51]. Nevertheless it is advantageous to use high optical powers because, under the fixed ratio  $|\mathcal{E}_1(0)/\mathcal{E}_{1s}(0)|$ , the larger  $\mathbf{E}_1$  is, the smaller are  $|\mathbf{d}_{31} \cdot \tilde{\mathbf{e}}_1(z_{\text{QW}})|$  and  $\alpha_1 \propto |\mathbf{d}_{31} \cdot \tilde{\mathbf{e}}_1(z_{\text{QW}})|^2$ , and therefore the larger are the gains Eqs. (30) and (33). For optical transition matrix elements of  $\sim 0.3$ –1 nm, small  $|\mathbf{d}_{31} \cdot \tilde{\mathbf{e}}_1(z_{\text{QW}})|$  can obviously be obtained by placing the QW active regions in cladding layers where the optical field decreases exponentially with growth of the distance from the confining layer. Such a waveguide design differs from that usually used in QW heterolasers, where the QW active region is placed near the maximum of the optical mode. Although this standard waveguide arrangement can also be employed here (under the condition of working with low enough pumping pulse peak powers  $\sim 4$ –40 mW, as pointed out at the beginning of this paragraph), as shown above, it is the proposed waveguide structure that can provide the maximal possible mid- far-ir gain (subject to one having a source of powerful enough and tightly focused optical pulses, certainly). It is important to stress here that, as the mid- to far-ir field spread in the  $z$  direction is much larger than that of the optical field, such a structure design by no means leads to the decrease of  $\alpha_2 \propto |\mathbf{d}_{32} \cdot \tilde{\mathbf{e}}_2(z_{\text{QW}})|^2$  and therefore long-wavelength gain reduction. For example, for the above determined relaxation rates and 1 ps driving pulses with the peak power of  $\sim 120$  W obtained in [50,51], this implies  $|z_{\text{QW}}| \approx 1.2$ –2  $\mu\text{m}$  for a 0.12  $\mu\text{m}$  thick confining layer; for 5 ps pulses with peak power 60 W and a 0.024  $\mu\text{m}$  thick confining layer, the corresponding  $|z_{\text{QW}}| \approx 7.3$ –10  $\mu\text{m}$ .<sup>6</sup> With these optimal parameters I obtain  $\alpha_1 \approx 0.15q \text{ cm}^{-1}$  for 120 W, 1 ps optical pulses, and  $\alpha_1 \approx 0.012q \text{ cm}^{-1}$  for 60 W, 5 ps pulses.

Then, I estimate the absorption coefficients for the optical and long-wavelength fields,  $\text{Im } k_1 \approx 0.25 \text{ cm}^{-1}$  [53] and

<sup>6</sup>In connection with these optical pulse powers, it is necessary to mention that estimates, based on the value of the GaAs two-photon absorption coefficient given in [52], show that in such a case the pump two-photon absorption length proves to be of the same order as its absorption length, due to linear absorption in the waveguide and excitation of QW electrons, so that further increase of the pump power appears unreasonable. On the other hand, moderate decrease of the pump powers in comparison with these figures [under the fixed ratio  $|\mathcal{E}_1(0)/\mathcal{E}_{1s}(0)|$  which, according to Eq. (36), determines the excited electron density in the third subband in the essential frequency interval of the  $3 \rightarrow 2$  transition responsible for the mid- to far-ir signal amplification] does not lead to a dramatic mid- to far-ir gain drop, whereas all the nonlinear effects diminish rather abruptly with decrease of pump intensity. So the following mid- to far-ir gain estimates obtained with neglect of the pump two-photon absorption remain true with order of magnitude accuracy.

$\text{Im } k_2 \approx 3.5 \text{ cm}^{-1}$  at  $\lambda_2 \approx 22 \mu\text{m}$  [32] and  $\text{Im } k_2 \approx 1.35 \text{ cm}^{-1}$  at  $\lambda_2 \approx 60 \mu\text{m}$  [29]. To estimate  $\alpha_2$ , I take for the long-wavelength matrix element a value of 3 nm [35,36] and evaluate the mid- to far-ir mode norm  $N_2$  by adjusting the results of [29] to the mid- to far-ir wavelengths  $\lambda_2 = 22$  or 60  $\mu\text{m}$  being considered here. So I get  $\alpha_2 \approx 1.47q \text{ cm}^{-1}$  for  $\lambda_2 = 22 \mu\text{m}$  and  $\alpha_2 \approx 0.086q \text{ cm}^{-1}$  for  $\lambda_2 = 60 \mu\text{m}$ . Such a quick drop of  $\alpha_2$  with increase of the mid- to far-ir field wavelength is due to the decrease of  $\omega_2 \propto 1/\lambda_2$  and the increase of  $|N_2|$  in the definition of  $\alpha_2$ , Eq. (28).

As follows from the numerical solution of the system (24) and (27), modified so as to take into account the above mentioned effect of the mid- to far-ir field absorption at  $\Delta \approx (0.3-1)\omega_2$ , at the optimal parameters found, the long-wavelength field can be amplified if the number of adjacent QWs  $q \geq 5$  for  $\lambda_2 = 22 \mu\text{m}$  and  $\geq 50$  for  $\lambda_2 = 60 \mu\text{m}$ .

Then, let me estimate the numerical values of the long-wavelength field gain starting with  $\lambda_2 = 22 \mu\text{m}$ . In this case, from the numerical solution, it follows that, even for a QW number  $q = 8$  only slightly exceeding the threshold value 5 found above the overall gain at  $x \approx 1.1 \text{ cm}$  ( $x_s \approx 2 \text{ cm}$ ) proves to be very large, so that the output peak mid-ir power at this point, calculated for the input long-wavelength peak power of  $\sim 0.1 \text{ W}$ , becomes comparable with the corresponding local peak power of the driving field ( $\sim 50 \text{ W}$ ); thus efficient conversion of the optical–mid-ir pulse takes place and all the above analysis, neglecting the optical signal extinction due to its conversion into the mid-ir field, becomes invalid. Nevertheless, from this analysis one can conclude that, for the optimal parameters found above, and even for a small adjacent QW number  $\geq 8$ , it is possible to amplify the 22  $\mu\text{m}$  mid-ir pulses up to peak powers of several tens of watts.

For  $\lambda_2 = 60 \mu\text{m}$ , again, the numerical solution of the system (24) and (27) shows that the gain quickly rises with increasing QW number over the above found threshold value 50. So, for  $q = 80$ , the optimal waveguide length (i.e., the length where the far-ir power reaches its maximum) is  $\sim 3 \text{ cm}$ , and the gain is approximately equal to 7 (which corresponds to  $\sim 50$ -fold amplification in power). This means that, using the input far-ir pulses with a peak power of  $\sim 0.2 \text{ mW}$  [27], this method can provide an output signal with  $\sim 10 \text{ mW}$  peak power at  $\lambda_2 = 60 \mu\text{m}$ . Further increase of the QW number, if technologically possible, leads to fast growth of the gain, whose calculation, however, requires taking into account the optical field variation over such a large QW set and its deviation from the optimal value determined above. So, for  $q = 90$ , the estimate of the output peak far-ir power around 30 mW (at the same input peak power of 0.2 mW), obtained without paying attention to the latter effect, is likely to be too optimistic, but nevertheless can give a notion of the fast gain growth with increasing QW number. The value 30 mW is much smaller than the input optical pulse peak power (60 W) so that for  $\lambda_2 = 60 \mu\text{m}$  this scheme is not able to provide efficient optical–far-ir pulse conversion.

It is worth noting here that in the case of a weak input mid- to far-ir pulse the detection of the corresponding output radiation (especially at  $\lambda_2 = 60 \mu\text{m}$ ) may present a difficult problem. In such a case, the accompanying optical field  $\mathbf{E}_3$  at

the carrier frequency  $\omega_3 \equiv \omega_1 - \omega_2$ , inevitably generated due to difference-frequency mixing of fields  $\mathbf{E}_1$  and  $\mathbf{E}_2$  on the  $2 \rightarrow 1$  transition or bulk second-order semiconductor nonlinearity, can in principle be used as an indicator of the mid- to far-ir emission. Unfortunately, in the present waveguide design, the coherence length  $\sim 1/|k_3 - k_1 + k_2|$  which, according to Eq. (12) (written for  $\mathbf{E}_3$ ), determines the efficiency of this process, proves to be  $\sim 10 \mu\text{m}$  at  $\lambda_2 = 22 \mu\text{m}$  and  $\sim 30 \mu\text{m}$  at  $\lambda_2 = 60 \mu\text{m}$ , i.e., much smaller than the characteristic length ( $\sim 1 \text{ cm}$  according to Fig. 4) where the field  $\mathbf{E}_2$  approaches its maximal value. Therefore, the output optical field  $\mathbf{E}_3$  should be much weaker than the mid- to far-ir one, and its use as an indicator of the  $\mathbf{E}_2$  field for the waveguide design considered in the paper seems to be impractical. Nevertheless, by means of special adjustments (not considered here) of the waveguide parameters, one can increase the coherence length for the  $\mathbf{E}_3$  field generation and thereby make its measurement a suitable tool for the mid- to far-ir signal detection.

#### IV. CONCLUSIONS

In conclusion, I show that a comparatively simple 2–3 cm long waveguiding QW heterostructure is able to convert an appreciable part of the optical pulse energy at  $\lambda_1 \sim 1 \mu\text{m}$  into a mid- to far-IR signal at  $\lambda_2 \sim 20$  or  $\sim 60 \mu\text{m}$  with approximately the same duration. This gives the possibility of producing even at room temperature mid- to far-ir

pulses with peak powers of several tens of watts (at  $\lambda_2 \sim 20 \mu\text{m}$ ) or several tens of milliwatts (at  $\lambda_2 \sim 60 \mu\text{m}$ ) for quite reasonable input optical peak power of  $\sim 100 \text{ W}$  and low mid- to far-ir beginning peak power levels of 100 and 0.1 mW, respectively, for the same wavelengths. The convenience of the present method is enhanced by the fact that the input optical and long-wavelength pulses may be taken as the output of a nonlinear mixing QW heterolaser [26,27], also working at room temperature and generating optical and difference-frequency mid- to far-ir fields in the mode-locking regime. Of course, employing input driving and long-wavelength pulses produced by other sources is also conceivable, and can be advantageous, allowing us to use more powerful driving signals and, therefore, to increase the mid- to far-ir pulse gain. One can also work with several such structures placed at some distance one after another, and introduce into each structure a new driving pulse at the moment when it is reached by the long-wavelength one. Employing such a cascade scheme allows us to solve the problem of the driving pulse extinction and to enhance even further the output mid- to far-ir pulse power.

#### ACKNOWLEDGMENTS

This research was supported by RFBR (Grants No. 05-02-17525 and 07-02-00486) and the Council for Support of the Leading Scientific Schools in Russia (Grant No. 4588.2006.2).

- 
- [1] D. Zimdars, J. A. Valdmanis, J. S. White, G. Stuk, S. Williamson, W. P. Winfree, and E. I. Madaras, in *Review of Progress in Quantitative Nondestructive Evaluation*, edited by D. O. Thompson and D. E. Chimenti, AIP Conf. Proc. No. 760 (AIP, Melville, NY, 2005), p. 570.
  - [2] E. Pickwell, B. E. Cole, A. J. Fitzgerald, M. Pepper, and V. P. Wallace, *Phys. Med. Biol.* **49**, 1595 (2004).
  - [3] T. Taniuchi, S. Okada, and H. Nakanishi, *J. Appl. Phys.* **95**, 5984 (2004).
  - [4] A. Agrawal, H. Cao, and A. Nahata, *New J. Phys.* **7**, 249 (2005).
  - [5] J. N. Heyman, R. Kersting, and K. Unterrainer, *Appl. Phys. Lett.* **72**, 644 (1998).
  - [6] B. H. Wu and J. C. Cao, *Physica B* **349**, 322 (2004).
  - [7] A. V. Maslov and D. S. Citrin, *J. Appl. Phys.* **93**, 10131 (2003).
  - [8] A. Dreyhaupt, S. Winnerl, T. Dekorsy, and M. Helm, *Appl. Phys. Lett.* **86**, 121114 (2005).
  - [9] L. Duvillaret, F.-F. Garet, J.-F. Roux, and J.-L. Coutaz, *IEEE J. Sel. Top. Quantum Electron.* **7**, 615 (2001).
  - [10] A. G. Davies, E. H. Linfield, and M. B. Johnston, *Phys. Med. Biol.* **47**, 3679 (2002).
  - [11] M. Hangyo, S. Tomozawa, Y. Murakami, M. Tonouchi, M. Tani, Z. Wang, K. Sakai, and S. Nakashima, *Appl. Phys. Lett.* **69**, 2122 (1996).
  - [12] C. Toth, J. van Tilborg, C. G. Geddes, G. Fubiani, C. B. Schroeder, E. Esarey, J. Faure, G. Dugan, and Wm. P. Lee-mans, *Proc. SPIE* **5448**, 491 (2004).
  - [13] D. H. Auston, K. P. Cheung, J. A. Valdmanis, and D. A. Kleinman, *Phys. Rev. Lett.* **53**, 1555 (1984).
  - [14] J. Singh, *IEEE Photonics Technol. Lett.* **8**, 488 (1996).
  - [15] *Semiconductor Lasers*, edited by E. Kapon (Academic Press, San Diego, 1999).
  - [16] *Intersubband Transitions in Quantum Wells: Physics and Devices*, edited by S. S. Li and Y.-K. Su (Kluwer, Boston, 1998).
  - [17] R. F. Kazarinov and R. A. Suris, *Sov. Phys. Semicond.* **5**, 707 (1971).
  - [18] J. Faist, F. Capasso, D. L. Sivco, C. Sirtori, A. L. Hutchinson, and A. Y. Cho, *Science* **264**, 553 (1994).
  - [19] F. Capasso, C. Gmachl, A. M. Tredicucci, A. L. Hutchinson, D. L. Sivco, and A. Y. Cho, *Opt. Photonics News* **10**, 33 (1999).
  - [20] S. Dhillon, J. Alton, S. Barbieri, C. Sirtori, A. de Rossi, M. Calligaro, H. E. Beere, and D. Ritchie, *Appl. Phys. Lett.* **87**, 071107 (2005).
  - [21] M. Hartig, J. D. Ganiere, P. E. Selbmann, B. Deveaud, and L. Rota, *Phys. Rev. B* **60**, 1500 (1999).
  - [22] M. C. Tatham, J. F. Ryan, and C. T. Foxon, *Phys. Rev. Lett.* **63**, 1637 (1989).
  - [23] L. E. Vorobjev, V. Yu. Panevin, N. K. Fedosov, D. A. Firsov, V. A. Shalygin, A. Seilmeier, S. R. Schmidt, E. A. Zibik, E. Towe, and V. V. KapaeV, *Semicond. Sci. Technol.* **21**, 1267 (2006).
  - [24] M. Zaluzny, *J. Appl. Phys.* **78**, 2868 (1995).

- [25] T. Unuma, M. Yoshita, T. Noda, H. Sakaki, and H. Akiyama, *J. Appl. Phys.* **93**, 1586 (2003).
- [26] A. A. Belyanin, F. Capasso, V. V. Kocharovskiy, V. V. Kocharovskiy, and M. O. Scully, *Phys. Rev. A* **63**, 053803 (2001).
- [27] V. A. Kukushkin, V. Ya. Aleshkin, A. A. Belyanin, A. A. Dubinov, V. V. Kocharovskiy, V. V. Kocharovskiy and M. O. Scully (unpublished).
- [28] C. Sirtori, A. Tredicucci, F. Capasso, J. Fais, D. L. Sivco, A. L. Hutchinson, and A. Y. Cho, *Opt. Lett.* **23**, 463 (1998).
- [29] M. Rochat, L. Ajili, H. Willenberg, J. Faist, H. Beere, G. Davies, E. Linfield, and D. Ritchie, *Appl. Phys. Lett.* **81**, 1381 (2002).
- [30] V. Berger and C. Sirtori, *Semicond. Sci. Technol.* **19**, 964 (2004).
- [31] *Introduction to Integrated Optics*, edited by M. K. Barnoski (Plenum Press, New York, 1974).
- [32] C. Sirtori, C. Gmachl, F. Capasso, J. Fais, D. L. Sivco, A. L. Hutchinson, and A. Y. Cho, *Opt. Lett.* **23**, 1366 (1998).
- [33] L. A. Vainshtein, *Electromagnetic Waves* (Soviet Radio, Moscow, 1988) (in Russian).
- [34] Y.-C. Chang and R. B. James, *Phys. Rev. B* **39**, 12672 (1989).
- [35] D. Bimberg, M. Grundmann, and N. N. Ledentsov, *Quantum Dot Heterostructures* (Wiley & Sons, New York, 1998).
- [36] *Semiconductor Lasers*, edited by E. Kapon (Academic Press, San Diego, 1999).
- [37] O. Madelung, *Semiconductors: Data Handbook* (Springer-Verlag, Heidelberg, 2003).
- [38] M. Altarelli, U. Ekenberg, and A. Fasolino, *Phys. Rev. B* **32**, 5138 (1985).
- [39] Ya. I. Khanin, *Fundamentals of Laser Dynamics* (Cambridge International Science Publishing, Cambridge, U.K., 2004).
- [40] A. Belyanin, C. Bentley, F. Capasso, O. Kocharovskaya, and M. O. Scully, *Phys. Rev. A* **64**, 013814 (2001).
- [41] M. Hartig, S. Haacke, P. E. Selbmann, B. Deveaud, R. A. Taylor, and L. Rota, *Phys. Rev. Lett.* **80**, 1940 (1998).
- [42] L. Allen and J. H. Eberly, *Optical Resonance and Two-Level Atoms* (Dover, New York, 1987).
- [43] U. Ekenberg, *Phys. Rev. B* **40**, 7714 (1989).
- [44] A. N. Pikhin and A. D. Yas'kov, *Sov. Phys. Semicond.* **12**, 622 (1978).
- [45] E. D. Palik, in *Handbook of Optical Constants of Solids*, edited by E. D. Palik (Academic Press, New York, 1985).
- [46] R. E. Fern and A. Onton, *J. Appl. Phys.* **42**, 3499 (1971).
- [47] H. C. Casey and M. B. Panish, *Heterostructure Lasers* (Academic Press, New York, 1978).
- [48] S. M. Goodnick and P. Lugli, *Phys. Rev. B* **37**, 2578 (1988).
- [49] D. J. Lockwood and Z. R. Wasilewski, *Phys. Rev. B* **70**, 155202 (2004).
- [50] G. Sangyoun, G. A. Alphonse, J. Connolly, P. J. Delfyett, *Proc. SPIE* **3384**, 12 (1998).
- [51] *Ultrafast Lasers: Technology and Applications*, edited by M. E. Fermann, A. Galvanauskas, and G. Sucha (Marcel Dekker, New York, 2001).
- [52] Y. J. Ding, *IEEE J. Sel. Top. Quantum Electron.* **10**, 1171 (2004).
- [53] V. Berger and C. Sirtori, *Semicond. Sci. Technol.* **19**, 964 (2004).